

# The London Study of Vortex States in a Superconducting Film Due to a Magnetic Dot

Serkan Erdin

Department of Physics, Northern Illinois University, DeKalb, IL, 60115  
& Advanced Photon Source, Argonne National Laboratory,  
9700 South Cass Avenue, Argonne, IL, 60439  
(November 18, 2018)

Here we report a study of vortex states in a thin superconducting film with a magnetic dot grown upon it by means of a method based on London-Maxwell equations. Vortices with single quantum flux ( $\Phi_0 = hc/2e$ ), giant vortices ( vortices with multiple flux ) as well as antivortices ( vortices with negative vorticity ) are taken into consideration. It turns out that giant vortices occur, when the dot's size is sufficiently smaller ( $R \leq 4.5\xi$ ) than the effective penetration depth  $\Lambda$ . In the case of a dot with sufficiently large size ( $R \geq 6\xi$ ), the vortices with single quantum flux dominate the vortex states. Their geometrical patterns are predicted up to seven vortices. Our calculations do not show the spontaneous appearance of antivortices.

PACS Number(s): 74.25.Dw, 74.25.Ha, 74.25.Qt, 74.78.-w

Type II superconductors are used in a wide variety of technological applications due to their high critical currents and fields [1]. In these superconductors, vortices appear when the magnetic field exceeds the first critical field  $H_{c1}$ . Under external current or field, vortices move, which causes the superconductor to switch to a resistive state. As a result, the system loses its superconductivity. Because of this, vortex pinning is quite important in applications of type II superconductors. One of the ways to pin vortices is to use the magnetic subsystems with either out-of-plane or in-plane magnetization. These subsystems are capable of trapping both vortices and antivortices, depending on the orientation and strength of their magnetization. The aforementioned systems are not only important for technological applications, such as devices that can be tuned by weak magnetic fields, but also offer rich physical effects which are not observed in the individual parts. Some of these effects were predicted elsewhere [2–7].

In the recent decade, magnetic dots growing on top of SC films have been extensively studied both experimentally [8] and theoretically [9,10]. In experimental studies, magnetic dots with in-plane magnetization are fabricated from Co, Ni, Fe, Gd-Co and Sm-Co alloys, whereas, for the dots with magnetization perpendicular to the plane, Co/Pt multilayers are used [11]. These studies report commensurability effects on transport properties, which confirm that the dots create and pin vortices. On theoretical side, several realizations of the aforementioned systems are analyzed through the Landau-Ginzburg framework and London theory. In these works, the authors investigated the conditions for vortices to appear and calculated their geometric configurations in equilibrium.

Recently, Priour *et al.* studied the vortex states of a SC

film with a magnetic dot array grown upon on it, through Ginzburg-Landau theory, and found several different configurations of vortices in the SC film [12]. Similar study was also done by Peeters *et al.*, but in the presence of a single dot [13,14]. One of the interesting results that is reported by these works is, when the dot's size is on the order of a few coherence lengths  $\xi$ , vortices with multiple flux quanta ( the giant vortices ) appear. The giant vortices are previously studied in the Landau-Ginzburg framework [15]. The stable antivortex (AV) ( vortices with vorticity opposite to vorticity of those trapped under the dot ) states were reported in similar systems [16]. The most interestingly, Kanda *et al.* recently reported the experimental evidence of the GV states and the other rearrangements of vortices in a mesoscopic SC disc, using the multiple-tunnel-junction method [17].

Earlier, we studied the vortex states due to a ferromagnetic (FM) dot with out-of-plane ( perpendicular to the film ) magnetization on top of a SC thin film [19]. In that work, we limited ourselves only to the vortices trapped under the dot, and calculated the equilibrium configurations, up to three vortices. However, in a more realistic picture, both vortices under the dot and antivortices outside the dot's boundaries can appear spontaneously, because total flux due to the magnetic dot over the entire infinite SC film is zero. Actually, this problem was studied for magnetic dipoles with out-of-plane magnetization [20]. Another interesting case is giant vortex (GV) states with multiple unit flux  $\Phi_0$ . In usual circumstances, it is hard to get vortices with multiple flux quanta, because their energy grows as the square of their vorticity. However, this energy cost can be overcome by the dots with radii of sufficiently less than effective penetration depth  $\Lambda = \lambda^2/d_{sc}$  [18], where  $\lambda$  is the London penetration depth and  $d_{sc}$  is the thickness of the SC film, and

with sufficiently large magnetization.

In this article, we focus on the complete picture together with antivortices and giant vortices, and aim to get analytical insight for the spontaneous vortex, antivortex and giant vortex states. For this purpose, we pursue the method based on London-Maxwell equations, which is fully developed elsewhere [19]. Though the London approach works well at the high  $\kappa = \Lambda/\xi$  limit, it perfectly serves our purpose and enables us to do analytical calculations. In our analytical and numerical calculations, we show that there are three regimes for the vortex states according to the dot's size. Namely, when the dot's size is sufficiently small, the GV states are dominant. If the dot's size is sufficiently large, we see only vortex states with single quantum flux (SQF). There is also an intermediate region in which both GV and SQF states appear. We calculate the geometrical configurations of SQF states in equilibrium up to seven vortices. In addition, our calculations do not show any AV states. At this point, we need to remark that the London framework might seem unreliable to some readers, when the ratio of the dot's size to the coherence length,  $\xi$ , is in the order of unity. However, one might expect that the vortices in the London framework, usually prefer staying in SQF states rather than GV states, since the London theory treats the vortex core as a point. Our approach then underestimates the dot's size, when the GV states appear. When the vortex cores are treated more accurately, as in Landau-Ginzburg framework, one might expect that the dot's size would be rather larger than that we estimate in this work. Nevertheless, the physics and qualitative result is still captured correctly in the London theory, although the results might be quantitatively different.

In the following section, we briefly introduce the method we follow in this article. Next, we study the giant vortex states with and without antivortices. The third section is devoted to a discussion on the SQF vortex states with and without AV states. The last section consists of the discussions and conclusions.

## I. METHOD

In order to attack this problem, we consider a thin circular magnetic dot of radius  $R$  with magnetization perpendicular to its plane at  $z = d$ , placed upon a thin SC film which both lay on the x-y plane  $z = 0$  (see Fig. 1). The dot's magnetization reads

$$\mathbf{m} = m\Theta(R - r)\delta(z - d)\hat{z}. \quad (1)$$

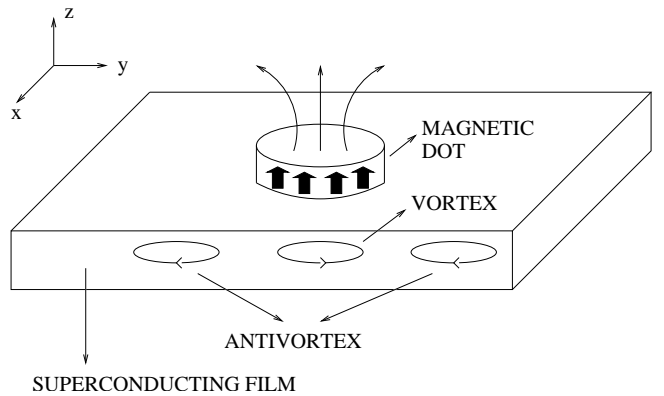


FIG. 1. Magnetic dot on a superconducting film.

The energy of the system in the presence of many vortices with arbitrary vorticities  $n_i$  is described elsewhere [19]. The appearance of  $N$  vortices with arbitrary positions  $\mathbf{r}_i$  in the system changes the energy by an amount:

$$\begin{aligned} \Delta_N = & \sum_{i=1}^N n_i^2 \varepsilon_v + \frac{1}{2} \sum_{i \neq j}^N n_i n_j \varepsilon_{vv}(r_{ij}) \\ & + \sum_{i=1}^N n_i \varepsilon_{mv}(r_i). \end{aligned} \quad (2)$$

Here  $\varepsilon_v = \varepsilon_0 \ln(\Lambda/\xi)$  is the self energy of a vortex without a magnetic dot,  $\varepsilon_0 = \Phi_0^2/(16\pi^2\Lambda)$ ,  $\varepsilon_{vv}$  is the vortex-vortex interaction, and  $\varepsilon_{mv}$  is the vortex-magnetic dot interaction. The vortex-vortex interaction reads

$$\varepsilon_{vv}(r_{ij}) = \frac{\varepsilon_0}{\pi} \left[ H_0\left(\frac{r_{ij}}{2\Lambda}\right) - Y_0\left(\frac{r_{ij}}{2\Lambda}\right) \right], \quad (3)$$

where  $r_{ij} = |\mathbf{r}_j - \mathbf{r}_i|$ ,  $H_0(x)$  and  $Y_0(x)$  are the Struve function of the zeroth order and the modified Bessel function of the second kind of the zeroth order, respectively [21]. The asymptotics of Eq.(3) are

$$\begin{aligned} \varepsilon_{vv} \approx & 2\varepsilon_0 \sum_{i>j} n_i n_j \ln \frac{\Lambda}{|\mathbf{r}_i - \mathbf{r}_j|}, |\mathbf{r}_i - \mathbf{r}_j| < \Lambda \\ \approx & 4\varepsilon_0 \Lambda \sum_{i>j} n_i n_j \frac{1}{|\mathbf{r}_i - \mathbf{r}_j|}, |\mathbf{r}_i - \mathbf{r}_j| > \Lambda. \end{aligned} \quad (4)$$

Note that in our further calculations, core energy  $\varepsilon_{core} \sim 0.809\varepsilon_0$  is renormalized to  $\Lambda$  in logarithmic terms. The vortex-magnetization interaction energy  $\varepsilon_{mv}$  is represented by

$$\varepsilon_{mv}(r_i) = -m\Phi_0 R \int_0^\infty \frac{J_1(qR)J_0(qr_i)e^{-qd}dq}{1 + 2\Lambda q}. \quad (5)$$

When  $d \neq 0$  and is significantly smaller than  $R$ , the correction to the  $\varepsilon_{vm}$  is on the order of  $d/R$ . Throughout the paper, we stick to  $d \ll R$  approximation to limit the number of parameters in our analytical calculations, which does not change the qualitative results. In our numerical calculations, however, we take  $d \neq 0$  to make sure that numerical integrations converge. The asymptotics at  $d = 0$  are

$$\begin{aligned}
\varepsilon_{vm} &\approx -m\Phi_0 R \sum_i n_i \left( \frac{1}{2\Lambda} - \frac{r_i^2}{8\Lambda R^2} \right), r_i < R < \Lambda \\
&\approx -m\Phi_0 R \sum_i n_i \left( \frac{1}{R} - \frac{3r_i^2\Lambda}{2R^4} \right), r_i < \Lambda < R \\
&\approx -m\Phi_0 R \sum_i n_i \frac{R^2\Lambda}{r_i^3}, R < \Lambda < r_i \\
&\approx -m\Phi_0 R \sum_i n_i \frac{R^2}{4\Lambda r_i}, R < r_i < \Lambda.
\end{aligned} \tag{6}$$

Additionally, under the assumption that the magnetization does not change direction due to its interaction with vortices, the self-magnetization energy is irrelevant to our calculations. Because of this, we do not take this energy into account. In the rest of the paper,  $\Delta_N$  denotes the energy of  $N$  vortices with single quantum flux ( $L = N$  state), while  $\Delta_N^g$  represents the energy of a giant vortex with vorticity  $N$  ( $L_g = N$  state).  $\Delta_N^{ga}$  is used for a GV with  $N$  vorticity and  $N$  SQF antivortex around it, whereas  $\Delta_N^a$  is used for  $N$  SQF states along with  $N$  AV states ( $L_a = N$  state).

## II. THE GIANT VORTICES

The self energy of a GV with vorticity  $n$  is proportional to its vorticity's square  $n^2$ , whereas the self energies of  $n$  vortices with SQF is just proportional to  $n$ . Because of this, GVs are unstable in usual superconductors. Even if they pop up, they decay into vortex states with vorticity  $n = 1$ . To get an idea about when GV states might occur, let us consider the following scenario in which SQF vortex states are trapped in a small region through a sufficiently small-sized magnetic dot so that they cannot go to further distances. In order for SQF states to be stable, the system requires more gain in energy, since energy grows due to the repulsion between SQF states when they get closer. For this purpose, the dot is required to have sufficiently high magnetization. We then expect the GVs can be stable if the dot's size is small enough and its magnetization is high enough. These physical arguments are our starting point. In this section, we consider a small circular dot  $R < \Lambda$ , placed upon a SC thin film. Previously, we studied the vortex states in the absence of antivortices and found that at first the  $L = 1$  state appears, and, with further increase of magnetization,  $L = 2, L = 3$  states occur in turn. In addition, the number of states depends on the magnetization and the dot's size. We anticipate the same situation when the dot's size is small enough to make the GV states stable. Contrary to our previous results, we expect  $L = 1, L_g = 2, L_g = 3$  and so on, when only GV states are present. The first question we ask here is how small does the dot have to be so that the  $L_g = n$  state will be preferred over the  $L = n$  state. The necessary conditions for this case are  $\Delta_n^g < \Delta_n$  and  $\Delta_n^g < 0$ . We first evaluate this problem analytically, and,

in doing so, we disregard the antivortices to simplify the calculations. They will be discussed at the end of this section. At the  $R < \Lambda$  limit, the effective energy of a GV state  $L_g = n$  reads

$$\Delta_n^g \approx n^2 \varepsilon_0 \ln \frac{\Lambda}{\xi} - \frac{nm\Phi_0 R}{2\Lambda}, \tag{7}$$

whereas the energy of  $L = n$  state is

$$\begin{aligned}
\Delta_n &\approx n\varepsilon_0 \ln \frac{\Lambda}{\xi} + 2\varepsilon_0 \sum_{i>j} \ln \left( \frac{\Lambda}{|\mathbf{r}_i - \mathbf{r}_j|} \right) \\
&\quad - \sum_i^n \frac{m\Phi_0 R}{2\Lambda} \left( 1 - \frac{r_i^2}{4R^2} \right),
\end{aligned} \tag{8}$$

where  $r_i$  is the position of  $i$ th antivortex from the dot's center. This problem can be simplified by using circular symmetry in the system. If the vortices are considered to be situated on a ring of radius  $r_v > \Lambda$  such that nearest vortices are equally distant from each other, the distance between  $i$ th and  $j$ th antivortices can be expressed as  $|\mathbf{r}_i - \mathbf{r}_j| = 2r_v |\sin(\pi(i-j)/n)|$ . Thereafter, taking the radius of the ring as  $r_v$ , the sum in the second term of Eq.(8) can be replaced by  $\sum_{k=1}^{n-1} (n-k) \ln(\Lambda/(2r_v \sin(\pi k/n)))$ . Under this assumption, the last term of Eq.(8) becomes  $(nm\Phi_0 R/2\Lambda)(1 - r_v^2/(4R^2))$ . Note that this assumption is valid for up to a few vortices. We expect that new rings occur as new vortices come out. In the next section, we show that the first ring carries 6 vortices on it. However this suffices for our analysis, since it is very unlikely to see a GV state with vorticity  $n = 6$ . As a result, the effective energy is now a function of  $r_v$ . Optimizing the effective energy with respect to  $r_v$ , we find its equilibrium value as

$$r_v = \sqrt{4(n-1) \frac{\varepsilon_0 R \Lambda}{m\Phi_0}}. \tag{9}$$

Directly substituting Eq.(9) into Eq.(8), we find

$$\begin{aligned}
\Delta_n &= n\varepsilon_0 \ln \frac{\Lambda}{\xi} + \frac{n(n-1)}{2} \varepsilon_0 \ln \left( \frac{\Lambda m\Phi_0 e}{16(n-1)R\varepsilon_0} \right) \\
&\quad - 2\varepsilon_0 \ln C_n - \frac{nm\Phi_0 R}{2\Lambda},
\end{aligned} \tag{10}$$

where  $C_n = \prod_{k=1}^{n-1} \sin(\pi k/n)^{n-k}$  and  $e = 2.71828$ . Let us compare Eq.(10) with the energy of a system in the presence of a GV with vorticity  $n$

$$\Delta_n^g \approx n^2 \varepsilon_0 \ln \frac{\Lambda}{\xi} - \frac{nm\Phi_0 R}{2\Lambda}. \tag{11}$$

From Eq.(11) and Eq.(10), we find

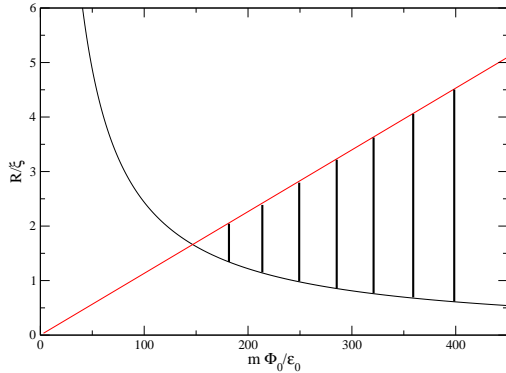
$$\frac{R}{\xi} < \frac{1}{\kappa} \frac{m\Phi_0}{\varepsilon_0} \frac{e}{16(n-1)C_n^{\frac{4}{n(n-1)}}}. \tag{12}$$

The above equation gives the upper limit for the dot's size as a function of magnetization of vorticity. When

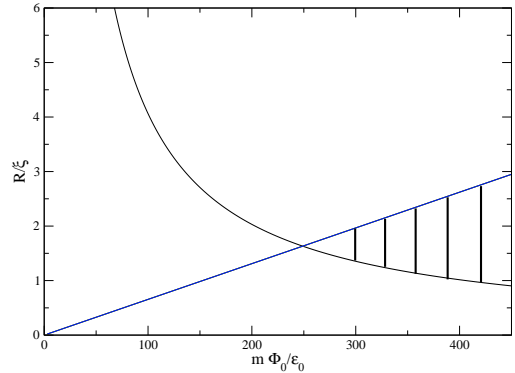
the dot's size is smaller than the upper limit, at first the  $L = 1$  state appears. The  $L_g = 2$  state follows next. With a further increase of magnetization, new GV states appear spontaneously. This picture is very similar to our previous results, except we have the GV states instead of the SQF states. In order for the  $L_g = n$  state to appear,

the necessary conditions are  $\Delta_n^g < \Delta_{n-1}^g$  and  $\Delta_n^g < 0$ . These conditions give us the lower limit as

$$\frac{R}{\xi} > \frac{2(2n-1)\kappa \ln \kappa}{\frac{m\Phi_0}{\varepsilon_0}}. \quad (13)$$



(a)  $L_g = 2$  vortex state

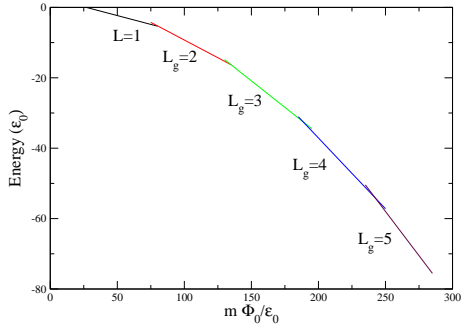


(b)  $L_g = 3$  vortex state

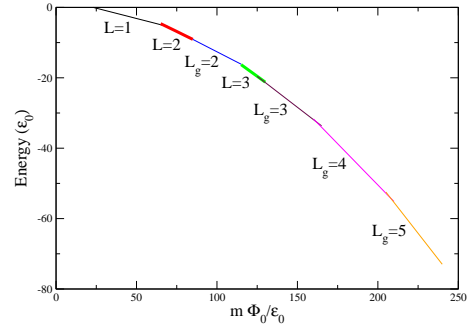
FIG. 2. The shaded regions show where  $L_g = 2$  and  $L_g = 3$  states can appear.

As seen from Fig. 2, as the vorticity of the GV states increases, the region in which they might appear shrinks. This suggests that the high vorticity GV states are more unlikely in usual circumstances. As a result of analytical calculations, we expect that the giant vortices can occur when  $R/\xi \sim 3, 4$ . To get the better result, we do numerical calculations for small values of  $R/\Lambda$  as analytical calculations suggest. In our numerical calculations, we set  $\kappa = 15$  and  $d/\Lambda = 0.05$ . The results of the numerical calculations are depicted in Fig. 3. We find that the giant vortices dominate the vortex states when  $R/\Lambda = 0.3$  ( $R/\xi = \kappa R/\Lambda = 4.5$ ). However, along with the further increase of the dot's size to 0.35 ( $R/\xi = 5.25$ ), we begin to see  $L = 2$  and  $L = 3$  states. However, we do not see  $L = 4$  or other states with a single quantum flux.

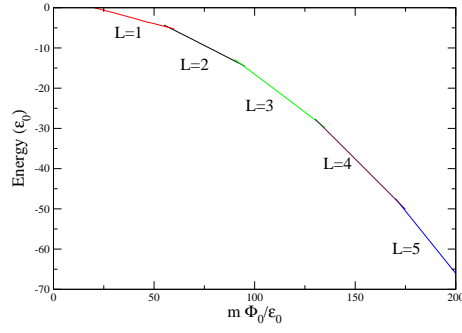
The physical reason for this is that the dot is still small enough so that the vortices can find the enough space to decay into SQF states. When the size is increased to 0.4 ( $R/\xi = 6$ ), we do not see any GV states anymore. The phase diagram of GV states is given in Fig. 4. The very bottom curve separates the no vortex region ( area below the curve ) from the region where the  $L = 1$  state becomes stable ( area between the 1st and 2nd curves). This curve is calculated from the equation  $\Delta_1 = 0$ . Next, the  $L_g = 2$  state follows. The corresponding curve, which separates the  $L = 1$  and  $L_g = 2$  states ( area between 2nd and 3rd curves ), is found from  $\Delta_2^g = \Delta_1$ . The following transitions are found from the equation  $\Delta_n^g = \Delta_{n-1}^g$  for  $n = 2, 3, \dots$



(a)  $R/\Lambda = 0.3$



(b)  $R/\Lambda = 0.35$



(c)  $R/\Lambda = 0.4$

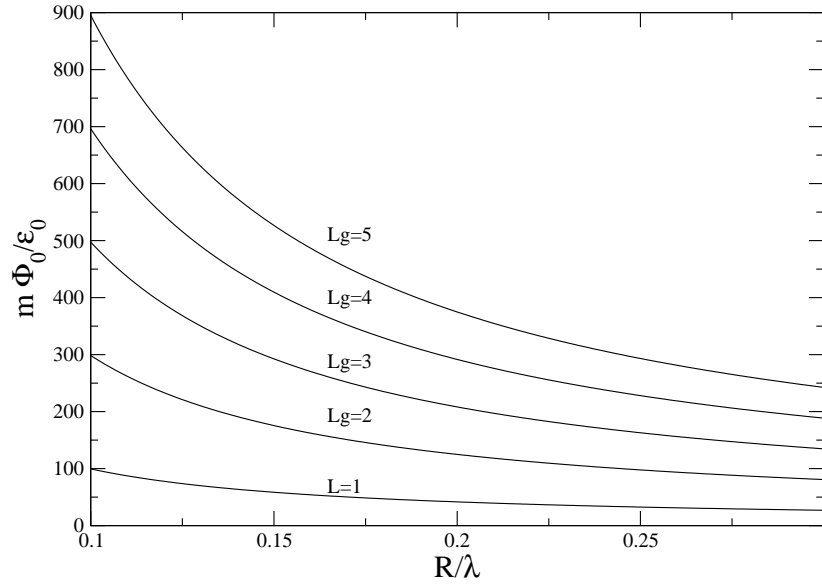


FIG. 4. Phase diagram of GV states.

Next, we consider the possibility of AV states together with GV states. The total flux due to the magnetic dot is zero throughout the entire SC film. The flux due to the dot causes the spontaneous appearance of GV or SQF states with the dot boundaries. By the same token, the flux due to the dot outside the dot boundaries might cause spontaneous AV states, when the dot's magnetic field penetrates into the the film. Since the total flux is zero over the entire SC film, we expect then the number of antivortices with single quantum flux equals the GV states's vorticity. In principle, the total GV's vorticity might differ from the number of SQF AV states in such a way that the net vorticity is positive. For the sake of simplicity, we do not consider this case. However, if stable AV vortices do not exist, this scenerio is quite unlikely. Because of circular symmetry, we assume that they are located on a ring of radius  $R < r_a < \Lambda$ . Again, we stress that this assumption is valid only for a few vortices. It is, however, sufficient to get a qualitative idea about AV states. Under the assumption that AV states are located within the region of  $\Lambda$  ( $r_a < \Lambda$  limit), the effective energy of a GV state  $L_g = n$  with  $n$  antivortices surrounding it reads

$$\Delta_n^{ga} \approx (n^2 + n)\varepsilon_v + n(n-1)\varepsilon_0 \ln \frac{\Lambda}{2r_a} - 2n^2\varepsilon_0 \ln \frac{\Lambda}{r_a} - 2\varepsilon_0 \ln C_n - \frac{nm\Phi_0 R}{2\Lambda} \left(1 - \frac{R}{2r_a}\right). \quad (14)$$

Minimizing the above equation with respect to the ring's radius  $r_a$ , we find

$$r_a = \frac{m\Phi_0 R^2}{4(n+1)\varepsilon_0 \Lambda}. \quad (15)$$

Directly substituting Eq.(15) into Eq.(14), we obtain

$$\Delta_n^{ga} = n(n+1)\varepsilon_0 \ln \left( \frac{2\kappa\varepsilon R^2 m\Phi_0}{(n+1)\Lambda^2 \varepsilon_0} \right) - 2\varepsilon_0 n^2 \ln 2 - 2\varepsilon_0 \ln C_n - \frac{nm\Phi_0 R}{2\Lambda}. \quad (16)$$

The GV state  $L_g = n$  is more energetically favorable than the  $L_{ga} = n$  state, when  $\Delta_n^{ag} < \Delta_n^g$  and  $\Delta_n^{ag} < 0$ . Using the initial approximation  $R < r_a < \Lambda$  and Eq.(15), we determine the boundaries of  $m\Phi_0/\varepsilon_0$  value as

$$4(n+1)\frac{\Lambda}{R} < \frac{m\Phi_0}{\varepsilon_0} < 4(n+1)\frac{\Lambda^2}{R^2}. \quad (17)$$

Next, we compare  $\Delta_n^{ga}$  and  $\Delta_n^g$  for several values of vorticity  $n$  within the limits of  $m\Phi_0/\varepsilon_0$  which are given in Eq.(17). It turns out than the giant vortices are always more favorable than the case in which they appear together with antivortices in  $R < r_a < \Lambda$  limit. At the opposite limit,  $r_a > \Lambda$ , it is quite unlikely to have stable states together with antivortices. Since the effective energy goes to  $n(n+1)\varepsilon_0 \ln \kappa - nm\Phi_0 R/(2\Lambda)$  when

$r_a \gg \Lambda$ . The energy difference  $n\varepsilon_0 \ln \kappa$  can be overcome only when  $R \sim \xi$ . However, we do not consider that case in this work because of the inaccuracy of London approximation at the small  $\kappa$  limit. Actually, when Eq.(2) is optimized together with antivortices, it manifests instability for vortex states, that is, high vorticity states become more favorable, and no low vorticity states appear. The reason for this is logarithmic divergence in the  $H_0(x) - Y_0(x)$  function. As  $x \rightarrow 0$ , this function goes logarithmically to infinity, which suggests that in the London approximation, a vortex-antivortex interaction is not taken care of accurately when the distance between the vortex-antivortex pairs is on the order of a few  $\xi$ . For this situation, we believe that the best approach is the nonlinear Landau Ginzburg equation.

### III. SQF VORTEX STATES

In the second section, we found that, when the dot's size is as large as about  $0.4\Lambda$  ( $6\xi$ ), only SQF vortex states occur. We devote this section to the analysis of geometrical patterns formed by SQF states and their phase diagram. In this part, we focus on two possible cases; vortices with and without antivortices. The former case has been previously analyzed for up to three vortices [19]. We determined the geometrical configurations of vortices in the ground state. Due to symmetry, the centers of the two vortices are located on a straight line connecting the vortices with the center of the dot at equal distances from the center. The occurrence of two vortices can be experimentally detected as a violation of circular symmetry of the field. For three vortices, the equilibrium configuration is a regular triangle. In this section, we consider further cases. Due to the circular symmetry, vortices seem to favor location on a circle such that they are equally distant from nearest neighbors. However, there is another possible case in which a vortex is situated at the dot's center while others are located on a circle as described just above, in the absence of antivortices.

In order for  $N$  vortices to appear, the necessary condition is that  $\Delta_N < 0$  and  $\Delta_N < \Delta_{N-1}$ . Using this criteria, we can determine in what configurations and order the vortices appear. To this end, we study only vortices with positive vorticity that are situated under the dot. The next step is to minimize with respect to the positions of vortices. We first start with one vortex. It turns out that it appears at the center of the dot.  $\Delta_1$  is a function of two dimensionless parameters  $m\Phi_0/\varepsilon_0$  and  $R/\Lambda$ .  $\Delta_1$  defines a critical curve that separates regions with or without vortices, as is depicted in Fig. 5. Next, we calculate  $\Delta_2$  for two vortices. Our calculations show that they are located on a straight line connecting the vortices with the center of the dot at equal distances from the center. The equation  $\Delta_2 = \Delta_1$  gives the second curve in Fig. 5, which separates the regions where one vortex and two vortices appear. That is, the area between the

first curve and second curve indicates where one vortex occurs, while the region between the second curve and third curve is for two vortices. The equilibrium configuration of three vortices is a regular triangle. A further increase of  $m\Phi_0/\varepsilon_0$  makes other vortex states more energetically favorable. Up to seven vortices tend to locate on a ring and equally distant from each other. Namely, four vortices form a square, whereas five vortices appear at the corners of a pentagon. The equilibrium configuration for six vortices is a hexagon. However, the seventh vortex appears at the dot's center, while the other six vortices form a hexagon around it. Geometrical patterns of up to seven vortices are depicted in Fig. 6. In principle, there exists an infinite series of such transitions. Here, we limit ourselves to seven vortices. The curves in a phase diagram of these seven vortices are obtained from  $\Delta_N = \Delta_{N-1}$  equation, which is a function of  $R/\Lambda$  and  $m\Phi_0/\varepsilon_0$ . Fixing the former, we calculate the latter variable. We do this for various values of  $R/\Lambda$ . Fitting the points that are obtained from numerical calculations, we find the generic function  $m\Phi_0/\varepsilon_0 \approx 4.22N/(R/\Lambda)^\nu$  where

$$\nu = 0.99 \pm 0.03.$$

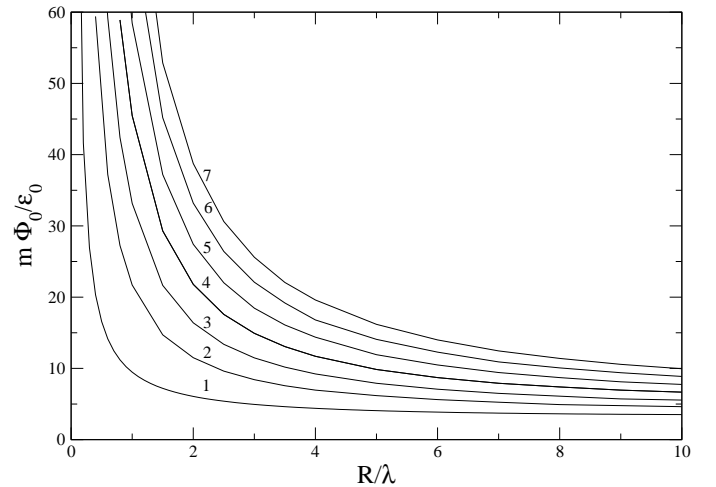


FIG. 5. Phase diagram of the vortex states.

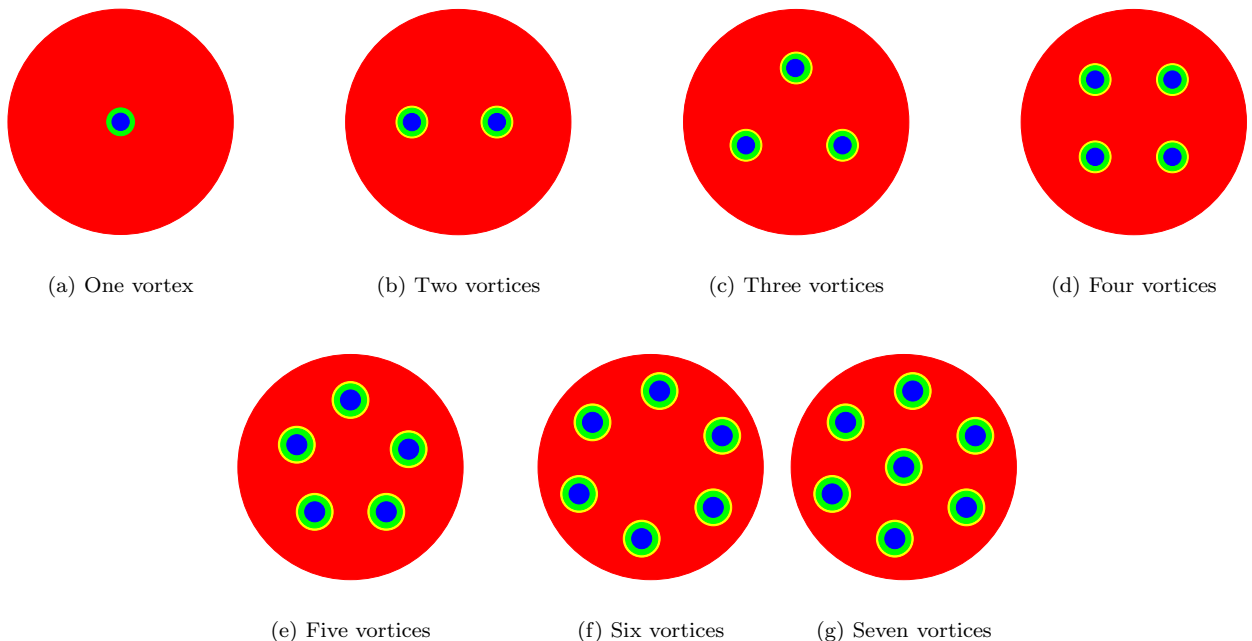


FIG. 6. Vortex states

Equilibrium positions of SQF states change significantly with increasing  $m\Phi_0/\varepsilon_0$ . That is, the larger  $m\Phi_0/\varepsilon_0$ , the more vortices are pushed towards the dot's center.

Next, we study SQF states in the presence of AV states.

First, we optimize Eq.(2) with respect to positions of vortices and antivortices. In our numerical calculation, we start from,  $R/\Lambda = 0.4$  and try larger values of  $R/\Lambda$ . We limit ourselves to the  $L_a = 2$  and  $L_a = 3$  states. Equilibrium configurations of  $L_a = 2$  and  $L_a = 3$  states are

depicted in Fig. 7. These configurations are independent of the dot's size, whereas equilibrium positions are dependent on  $m\Phi_0/\varepsilon_0$ . The further increase of this parameter causes the further push of vortices towards the dot's center, and antivortices away from the dot's boundaries. As seen in Fig. 7, antivortices are aligned with vortices and appear on a ring outside the dot. Next, we compare the

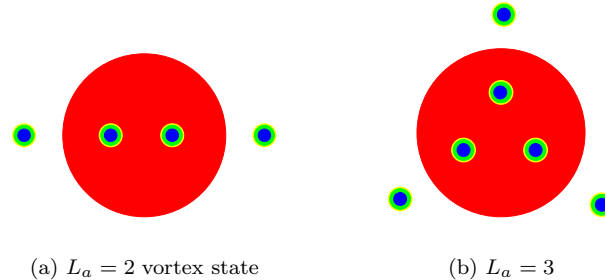


FIG. 7. Equilibrium configurations of  $L_a = 2$  and  $L_a = 3$  states.

#### IV. CONCLUSIONS

We studied the vortex states that occur spontaneously in the ground states of a SC thin film with a single FM dot grown upon it, in the London approximation. Our calculations showed that GV states are more energetically favorable when the dot's size is up to  $0.3\Lambda$  ( $4.5\xi$ ). Between  $R = 0.3\Lambda$  ( $4.5\xi$ ) and  $R = 0.4\Lambda$  ( $6\xi$ ), both GV and SQF states appear. Beyond  $0.4\Lambda$  ( $6\xi$ ), only SQF states are stable.

Furthermore, we determine the geometric patterns of up to seven vortices. Our results show that vortices form regular geometric patterns, such as a regular triangle, square, pentagon and hexagon. However, in the case of seven vortices, one vortex occurs at the dot's center, while other six sit at the corners of a hexagon. The phase diagram of SQF vortex states obeys an equation  $N/(R/\Lambda)$ , which suggests that high-vorticity states prefer larger dots.

We also studied the cases together with AV states. However, our calculations did not show any stable vortex states together with antivortices. This result might seem implausible since one would expect the presence of AV states due to the zero flux condition over the entire film. However, the zero flux condition can also be satisfied by the presence of a supercurrent outside the dot boundaries, which circulates in the opposite direction to the currents created by vortices under the dot. Furthermore, the London approach does not enable us to analyze the vortex and antivortex states when the dot's size is as large as a few  $\xi$ , because it fails for distances on the order of coherence length. This failure is significantly transparent in the presence of AV states. However, positive vorticity states can be studied through the London approach.

In closing, we studied SQF vortex, GV and AV states

effective energies of these states with SQF states without antivortices around them. The comparison of effective energies with and without AV states shows that AV states are not energetically favorable. However, as discussed in the previous section, for dots whose size is on the order of a few  $\xi$ , there might be stable AV states. However, the London theory does fail in that case.

due to a magnetic dot in the London approximation. Experimentally, these states can be checked by magnetic force microscopy techniques.

#### V. ACKNOWLEDGMENTS

The author acknowledges Valery L. Pokrovsky for his very fruitful discussions. The most of this work was done during my stay at the University of Minnesota and was partially supported by the U.S. Department of Energy, Office of Science, under Contract No. W-31-109-ENG-38.

- 
- [1] M. Tinkham, *Introduction to Superconductivity* 2nd. ed. Dover Publications 2004.
  - [2] I.F. Lyuksyutov and V.L. Pokrovsky, Phys. Rev. Lett. **81**, 2344 (1998).
  - [3] S.Erdin, I.F. Lyuksyutov, V.L. Pokrovsky and V.M. Vinokur, Phys. Rev. Lett. **88**, 017001 (2002).
  - [4] S. Erdin, Physica C **391**,140 (2003).
  - [5] S. Erdin, Phys. Rev. B **69**, 214521 (2004).
  - [6] M.A. Kayali and V.L. Pokrovsky, Phys. Rev. B **69**, 132501 (2004).
  - [7] V.L. Pokrovsky and H. Wei, Phys. Rev. B **69**, 104530 (2004).
  - [8] Y. Nozaki, Y. Otani, K. Runge, H. Miyajima, B. Pannetier, J.P. Nozieres and G. Fillion, J. Appl. Phys. **79**, 8571 (1996); M.J. Van Bael, K. Temst, V.V. Moshchalkov and Y. Bruynseraede, Phys. Rev. B **59**, 14674 (1999); M. Baert, V.V. Metlushko, R. Jonckheere, V.V. Moshchalkov and Y. Bruynseraede Phys. Rev. Lett. **74**, 3269 (1995).



- [9] I.F. Lyuksyutov and V.L. Pokrovsky, *Adv. Phys.* **54**, 67 (2005).
- [10] S. Erdin, *Frontiers in Superconducting Materials*, edited by A. Narlikar, (Springer-Verlag, New York,2005),pp. 425-458.
- [11] M.J. Bael, L. Van Look, K. Temst et al. *Physica C* **332**, 12 (2000).
- [12] D.J. Priour Jr. and H.A. Fertig, *Phys. Rev. Lett.* **93**, 057003 (2004).
- [13] I.K. Marmoros, A. Matulis and F.M. Peeters, *Phys. Rev. B* **53**, 2677 (1996).
- [14] M.V. Milosevic and F.M. Peeters, *Phys. Rev. B* **68**, 024509 (2003).
- [15] V. Hakim, A. Lemaitre and K. Mallick, *Phys. Rev. B* **64**, 134512 (2001).
- [16] Milosovic M.V., Yampolskii S.V. and Peeters F.M., *Phys. Rev. B* **66**, 174519 (2002).
- [17] A. Kanda, B.J. Baelus, F.M. Peeters, K. Kadowaki and Y. Ootuka, *Phys. Rev. Lett.* **93**, 257002 (2004).
- [18] A.A. Abrikosov, *Introduction to the Theory of Metals* North Holland, (1986).
- [19] S. Erdin, A.M. Kayali, I.F. Lyuksyutov and V.L. Pokrovsky, *Phys.Rev. B* **66**, 014414 (2002).
- [20] M.V. Milosevic, S.V. Yampolskii, and F.M. Peeters, *Phys Rev. B* **66**, 174519 (2002).
- [21] M. Abramowitz and I.A. Stegun, *Handbook of Mathematical Functions*, Dover Publications (1970).